 Cytometry 37:14–20 (1999)

Correlating Cell Cycle With Metabolism in Single Cells: Combination of Image and Metabolic Cytometry

Sergey N. Krylov, Zheru Zhang, Nora W.C. Chan, Edgar Arriaga, Monica M. Palcic, and Norman J. Dovichi*

Department of Chemistry, University of Alberta, Edmonton, Alberta, Canada

Received 5 March 1999; Revision Received 4 May 1999; Accepted 4 May 1999

Background: We coin two terms: First, chemical cytometry describes the use of high-sensitivity chemical analysis techniques to study single cells. Second, metabolic cytometry is a form of chemical cytometry that monitors a cascade of biosynthetic and biodegradation products generated in a single cell. In this paper, we describe the combination of metabolic cytometry with image cytometry to correlate oligosaccharide metabolic activity with cell cycle. We use this technique to measure DNA ploidy, the uptake of a fluorescent disaccharide, and the amount of metabolic products in a single cell.

Methods: A colon adenocarcinoma cell line (HT29) was incubated with a fluorescent disaccharide, which was taken up by the cells and converted into a series of biosynthetic and biodegradation products. The cells were also treated with YOYO-3 and Hoechst 33342. The YOYO-3 signal was used as a live-dead assay, while the Hoechst 33342 signal was used to estimate the ploidy of live cells by fluorescence image cytometry. After ploidy analysis, a cell was injected into a fused-silica capillary, where the cell was lysed. Fluorescent metabolic products were then separated by capillary electrophoresis and detected by laser-induced fluorescence.

Results: Substrate uptake measured with metabolic cytometry gave rise to results similar to those measured by use of laser scanning confocal microscopy. The DNA ploidy histogram obtained with our simple image cytometry technique was similar to that obtained using flow cytometry. The cells in the G_1 phase did not show any biosynthetic activity in respect to the substrate. Several groups of cells with unique biosynthetic patterns were distinguished within G_2/M cells.

Conclusions: This is the first report that combined metabolic and image cytometry to correlate formation of metabolic products with cell cycle. A complete enzymatic cascade is monitored on a cell-by-cell basis and correlated with cell cycle. Cytometry 37:14–20, 1999.

Key terms: chemical cytometry; metabolic cytometry; capillary electrophoresis; oligosaccharide metabolism

Chemical cytometry is our term for the analysis of the chemical composition of single cells. In 1953, Edstrom reported the first chemical cytometry analysis, where fine silk fibers were used for the electrophoretic determination of RNA contained within a single cell (1). In 1965, Maholi and Niewisch used a fine agarose fiber to perform gel electrophoresis separation of hemoglobin in single erythrocytes (2). In 1987, Jorgenson lysed a single cell and fluorescently labeled its contents in a miniature reaction vial (3,4). The reaction products were then injected into a capillary chromatography column for analysis. In 1994, Ewing greatly simplified the procedure by injecting the cell directly into the separation capillary, where lysis and labeling were performed on-column (5). Workers have studied single erythrocytes and neurons (6–15). An extension of the single-cell work involves study of exocytosis from single pancreatic cells or neurons (16–23). Recently, there has been interest in mass spectrometric identification of proteins from single cells (24–26). In most cases, chemical cytometry was used to analyze endogenous components within the cell; in one case, a single enzyme's activity was monitored (15).

In earlier work, we studied cell extracts prepared from $\approx 10^6$ cells grown in the presence of a tetramethylrhodamine-labeled disaccharide (27). The disaccharide was taken up by the cells where it acted as a substrate for an enzymatic cascade, forming biosynthetic products corresponding to larger oligosaccharides and biodegradation products corresponding to the monosaccharide and the fluorescently labeled linker. The fluorescent tag associated with the substrate survived many of the metabolic transformations. When separated with a high-resolution capillary electrophoresis system and detected with a high-sensitiv-

Grant sponsor: National Sciences and Engineering Research Council.

*Correspondence to: Professor Norman J. Dovichi, Department of Chemistry, University of Alberta, Edmonton, Alberta T6G 2G2, Canada.
E-mail: norm.dovichi@ualberta.ca

ity laser-induced fluorescence detector, minute amounts of metabolic product were detected in the cellular extracts. We reported the detection of ~50 molecules ($\sim 8 \times 10^{-23}$ mole = 80 yoctomole = 80 ymol) of metabolic product (28,29).

The high sensitivity of our fluorescence detector suggests that metabolic products can be detected in single cells. In this paper, we describe metabolic cytometry, which is the use of capillary electrophoresis/laser-induced fluorescence to analyze the metabolic products within single cells. Five metabolic products were separated and identified from the single cells. We combine this metabolic cytometry with an image cytometry system to provide a hybrid method that monitors cell cycle, substrate uptake, and biosynthetic and biodegradation pathways in single cells.

METHODS

Cell Culture

The HT29 cell line (human colon adenocarcinoma) was grown to 80% confluence in Dulbecco's modified Eagle's medium, supplemented with 10% fetal calf serum and 40 μg/mL gentamycin at 37°C in 5% CO_2 atmosphere. The cells were then incubated for 18 h with 25 μM tetramethylrhodamine-labeled βGal(1→4)βGlcNAc substrate (LacNAc-TMR). A long incubation time is required because of the low penetration rate of the LacNAc-TMR substrate through the cellular membrane. After incubation, the cells were washed eight times with phosphate-buffered saline (PBS) to remove the residual substrate. The cells were resuspended in PBS.

Cell Extract

To prepare cell extracts, 2×10^6 cells were homogenized in a micro-tissue grinder on ice with 20 strokes every 15 min over a 1.5 h period. The sample was centrifuged to remove cellular debris. The supernatant was loaded onto a C-18 Sep Pak cartridge and washed with water. The hydrophobic TMR-labeled compounds were eluted from the cartridge with high performance liquid chromatography (HPLC) grade methanol. The methanol was evaporated and the residue was dissolved in 160 μL of the electrophoresis running buffer.

Image Cytometry and Cell Cycle Measurement

A 0.1 mM YOYO-3 (λ_{ex} = 612 nm, λ_{em} = 631 nm) stock solution was prepared in water and stored at −18°C. A 1-mg/mL stock solution of Hoechst 33342 (λ_{ex} = 350 nm, λ_{em} = 461 nm) was prepared in water and stored at 4°C. YOYO-3 and Hoechst 33342 were added to the cell suspension (10^6 cells/mL) to make final concentrations of 1 μM and 10 μg/mL, respectively. Cells were incubated for 1 h at 37°C before analysis. This incubation time provided proportional staining of DNA; the cytotoxic effect of Hoechst 33342 was not significant. A 1-μL aliquot of the cell suspension was diluted with 50 μL of PBS buffer, and this diluted suspension was placed on a glass microscope slide. YOYO-3 dye intercalates DNA only in dead cells. We excluded the cells with YOYO-3 fluorescence from further analysis. A live cell was centered in the field of view of the 125× objective on a microscope equipped with an R1635–02 photomultiplier tube. The PMT shutter was opened, focusing was adjusted to maximize the Hoechst signal, and the signal was recorded.

Metabolic Cytometry

A 45-cm long, 19-μm ID, and 144-μm OD fused-silica capillary (Polymicro, Phoenix, AZ) was placed over a cell using micromanipulators (Model MX630R, Newport Bio-Instrument, Nepean, ON) and with the aid of an inverted microscope (Model IMT-2, Olympus America Inc., Melville, NY). An 11-kPa partial vacuum was applied to the distal end of the capillary for 1 s, drawing the cell approximately 0.2-mm within the capillary. The capillary tip was placed in a vial containing the sodium dodecyl sulfate (SDS)–running buffer (10 mM of each: SDS, sodium phosphate, sodium tetraborate, and phenylboronic acid, pH 9.3) which lysed the cell within 20 s.

The separation was performed using a locally constructed capillary electrophoresis instrument described in detail elsewhere (29). The electrophoresis was driven by a CZE1000R high-voltage power supply (Spellmann, Plainview, NY) at 18 kV. The power supply was controlled with a Macintosh Quadra 650 computer via an NB-MIO-16XH-18 input/output board (National Instruments, Austin, TX, USA). This board was also used to record the electrical current and fluorescence intensity as functions of time during the electrophoretic separation.

Our fluorescence detector used 1-mW helium-neon laser (Melles Griot, Nepean, ON) emitting at 543.5 nm. The laser beam was focused with 6.3× objective (Melles Griot) into the sheath flow cuvette (NSG, New York). The capillary was inserted in a locally constructed sheath-flow cuvette so that the laser beam was approximately 20 μm below the tip of the capillary. The cuvette was similar to one manufactured by Ortho Diagnostics around 1980 (model 300–0511–000). Our cuvette had a 200 μm square flow chamber with 1-mm-thick quartz windows. Sheath-flow through the cuvette was created by a simple siphon system, and the sheath-flow buffer was the same as used for the separation.

The polyimide coating was removed from the last ≈2-mm portion of the capillary to reduce background fluorescence from the coating. Analyte fluorescence was collected at 90° with respect to the incident laser beam using a 60× 0.7 N.A. microscope objective Model 60X-LWD (Universe Kogaku, Oyster Bay, NY) and spectrally filtered with interference filter centered at 580 nm and having 30 nm bandwidth (Omega Optical, Brattleboro, VT). Fluorescence was detected with an R1477 photomultiplier tube (PMT; Hamamatsu, Bridgewater, NJ).

Standard solutions of LacNAc-TMR were used to calibrate the optical detection system. The mass detection limit of the instrument was determined to be 100 TMR-labeled molecules (30–33).

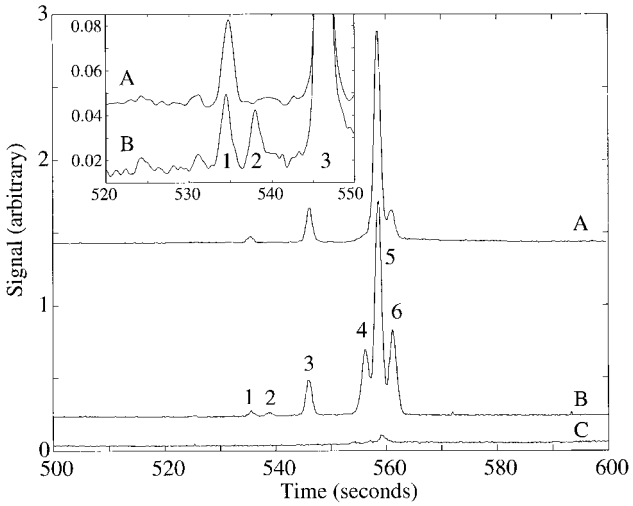

FIG. 1. Electropherograms of TMR-labeled species obtained from a single HT29 cell (curve A), an HT29 extract (curve B), and the PBS buffer used to resuspend the cells (curve C). The inset shows peaks 1–2 for the single cell and cell extract.

Confocal Microscopy

The fluorescence intensity of 65 cells, chosen at random, was measured by confocal microscopy. Images were obtained with a MultiProbe 2001 confocal laser-scanning microscope (Molecular Dynamics). A 4-mW argon-krypton ion laser at 568 nm was used as the excitation source. The total fluorescence intensity was estimated by imaging 32 sections through the cells and summing the intensity through each cell. A step-size between sections was 0.7 μm to accurately estimate the cell's fluorescence.

Flow Cytometry

Conventional flow cytometry data was generated for cells that had been incubated with both LacNAc-TMR and Hoechst 33342. These conditions were chosen to be similar to that used for metabolic cytometry experiments. A Coulter Elite flow-cytometer was used to generate the data.

RESULTS

Metabolic Cytometry

Figure 1 presents electropherograms generated from a single HT29 cell, an HT29 cell extract, and a control consisting of the resuspension buffer. Six peaks were observed in the single-cell and cell extract electropherograms, forming the metabolic profile. We were concerned that the metabolic cytometry profile might be biased by injection of fluorescent contaminants in the buffer used to resuspend the cells. However, only a very small peak was observed in the control electropherogram; any resuspension buffer injected with a cell makes a minute contribution to the metabolic profile.

Most peaks were identified in the cell extract profile based on co-migration with authentic standards and by enzymatic hydrolysis. Peak 1 was identified as a tetrasaccharide Le^y, αFuc(1→2)βGal(1→4)[α Fuc(1→3)]βGlcNAc-TMR, formed by α1→2 and α1→3 fucosylation of the disaccharide substrate. Peak 2 was a trisaccharide Le^x, βGal(1→4)[αFuc(1→3)]βGlcNAc-TMR, formed by addition of fucose to the LacNAc-TMR substrate by α1→3 fucosyltransferase. Peak 3 was the substrate. Peak 4 did not co-migrate with any of our standards. Peak 5 was βGlcNAc-TMR, formed by β-galactosidase activity on the substrate. Peak 6 co-migrated with TMR-aglycone, $(HO(CH_2)_8CONH(CH_2)_2NH\text{-TMR})$, which is produced by hydrolysis of the LacNAc-TMR substrate by sequential action of β-galactosidase and hexosaminidases; however, we have not enzymatically confirmed this peak's identity. The protocol for peak identification will be described elsewhere. Substrate uptake was estimated by summing the intensity of the six peaks:

$$\text{uptake} = \sum_{i=1}^{6} \text{peak}\,(i). \qquad (1)$$

Uptake was also estimated by confocal microscopy. We assume that metabolism neither destroys the fluorescent label nor changes the spectroscopic properties of the label. In metabolic cytometry, substrate uptake was estimated by summing the intensity of all peaks in the electropherogram. The 45% relative standard deviation ($n = 20$) in cell-to-cell intensity from metabolic cytometry was indistinguishable from a 43% relative standard deviation ($n = 65$) in cell-to-cell fluorescence intensity measured by confocal microscopy. Metabolic cytometry and image cytometry provided similar results for substrate uptake. The high relative standard deviation of substrate uptake can be due to cell-to-cell variation in cell size and cellular membrane permeability for the substrate. These may be associated with cells being in different phases of the cell cycle.

Conventional cytometric methods are unable to distinguish between metabolic products. In contrast, metabolic cytometry provides a detailed profile of enzymatic activity for each cell. Six metabolic profiles were chosen to illustrate the range of behaviors (Fig. 2). Cell A has low substrate uptake but generates the largest relative amounts of both the aglycone degradation product and the Le^y biosynthetic product. In contrast, cells E and F have the largest uptake of the substrate, which is almost completely converted to βGlcNAc-TMR, with virtually no evidence for other biotransformations.

Image Cytometry

Cells were treated with two DNA intercalating dyes in addition to the LacNAc-TMR substrate. YOYO-3 is permeant only to dead cells and emits red fluorescence upon excitation at 600 nm. Only live cells were chosen for further study.

Hoechst 33342 is permeant to live cells and emits blue fluorescence upon excitation at 350 nm. The intensity of the Hoechst 33342 fluorescence was measured with a photomultiplier tube connected to the microscope. Figure

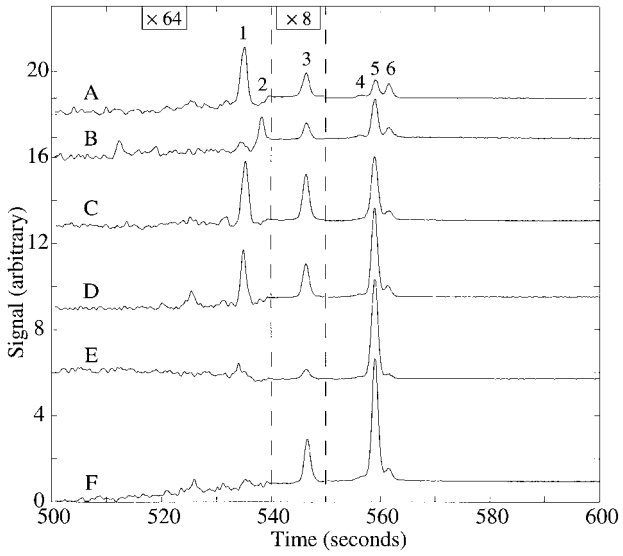

FIG. 2. Single cell metabolic profiles from six cells. The electropherograms were offset for clarity. The region from 540 to 550 s was expanded by a factor of 8 and the region from 500 to 540 s was expanded by a factor of 64.

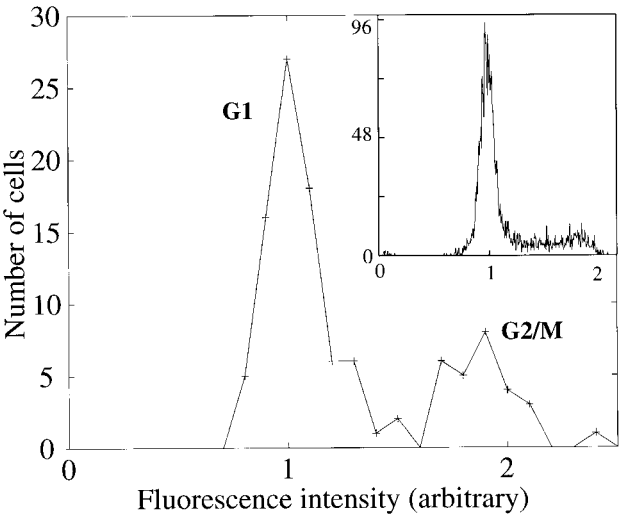

FIG. 3. Histogram of DNA content from 108 randomly chosen cells measured with an inverted microscope. The inset shows data generated by a conventional flow cytometer.

3 presents a frequency histogram for DNA content obtained for 108 randomly chosen cells. The inset shows flow cytometry data generated from 3684 cells from the same culture. Both distributions showed two peaks corresponding to cells in the G_1 and G_2/M phase of the cell cycle. The coefficient of variation in fluorescence signal for the G_1 cells was 12% for our image cytometry data and 10% for the commercial flow cytometer.

We used this technique to choose only G_1 and G_2/M cells for our metabolic cytometry analysis. We applied metabolic cytometry to analyze 20 cells in the G_1 phase and 23 cells in the combined G_2/M phase.

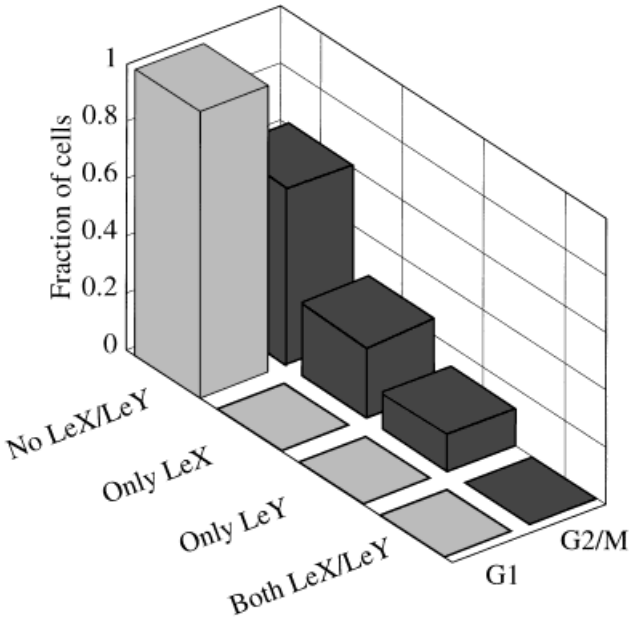

FIG. 4. Fraction of cells showing biosynthesis. G_1 cells showed no biosynthesis, whereas ≈40% of G_2/M cells showed biosynthesis of either Le^X or Le^Y, but not both.

Combined Metabolic Cytometry and Image Cytometry

Biosynthesis. Biosynthetic activity is defined as the fraction of uptake due to biosynthetic peaks (peaks 1–2):

$$\text{biosynthetic activity} = \frac{\Sigma \text{ biosynthetic peaks}}{\text{uptake}}. \quad (2)$$

No biosynthetic activity was observed in the G_1 cells (Fig. 4). Based on the sensitivity of our instrument, less than 100 molecules of biosynthetic product were present within these cells.

The G_2/M cells could be divided into classes based on their biosynthetic activity. No biosynthetic products were observed in about 60%of the G_2/M cells. Again, these cells had less than 100 molecules of biosynthetic product.

However, a fraction of the G_2/M cells were biosynthetically active. One class generated only Le^x, another generated Le^y. No cells in this study generated measurable amounts of both biosynthetic products. About 25% of the G_2/M cells generated measurable amounts of Le^x, about 12%of the G_2/M cells generated measurable amounts of Le^y, and the remainder had no detectable biosynthetic products. The extent of biosynthesis was small, with an average of roughly 3000 molecules of product in those cells, which accounts for 4% of the fluorescent compounds within the cell. For subsequent analysis, we divided the cells into three classes: G_1, biosynthetically inactive G_2/M, and biosynthetically active G_2/M.

Uptake. Uptake (total amount of rhodamine-labeled species in the cell) was determined along with cell cycle. Cells in the G_1 phase had an average of ≈25,000 fluores-

cent molecules. The biosynthetically inactive cells had an average of ≈50,000 fluorescent molecules. The biosynthetically active G_2/M cells had an average of ≈90,000 fluorescent molecules.

Biodegradation. Biodegradation activity is defined as the fraction of uptake due to biodegradation peaks (peaks 4–6):

$$\text{biodegradation activity} = \frac{\Sigma \text{ biodegradation peaks}}{\text{uptake}}. \quad (3)$$

The unknown component, peak 4 , is assumed to be a biodegradation product because of its relatively long migration time. Biodegradation dominated the metabolic activity for all cells, accounting for ≈80% of the fluorescent signal.

Biodegradation proceeds through several steps. First, β-galactosidase removes one monosaccharide from the disaccharide substrate, producing the monosaccharide βGlcNAc-TMR. Subsequent degradation by hexosaminidase produces the aglycone, which consists of a linker-arm that is connected to the fluorescent label.

Biodegradation is dominated by the action of β-galactosidase to produce βGlcNAc-TMR, peak 5. On average, βGlcNAc-TMR accounted for about 65% of the fluorescent signal for all cell classes. The aglycone, peak 6, accounted for an additional 15% of the signal for all cell classes.

Peak 4 remains unidentified. Its relative amount was negatively correlated with total substrate uptake ($r = -0.63$, $n = 43$, $P = 0.6 \times 10^{-6}$). However, this negative correlation obscures the behavior of different cell populations (Fig. 5). The peak was present at very low concentration in G_2/M phase cells undergoing biosynthesis, accounting for 1% of the fluorescent signal. It was present at higher concentration in the biosynthetically inactive G_2/M cells, accounting for 3% of the fluorescent signal. The compound was present at highest concentration in the G_1 cells, accounting for 6% of the fluorescent signal.

Metabolic activity. Metabolic activity is the sum of biosynthetic and biodegradation activity:

$$\text{metabolic activity} = \frac{\Sigma \text{ biosynthetic peaks}}{\text{uptake}} + \frac{\Sigma \text{ biodegradation peaks}}{\text{uptake}}. \quad (4)$$

The average metabolic activity was 0.87 ± 0.08 for the G_1 cells, 0.84 ± 0.08 for the biosynthetically inactive G_2/M cells, and 0.84 ± 0.08 for the biosynthetically active G_2/M cells (Fig. 6). Thus, the average metabolic activity was equal within the limits of experimental error for the three groups of cells. The products of biodegradation constituted more than 90% of the total metabolites and was independent of the cell cycle.

Metabolic activity was uncorrelated with substrate uptake for G_1 cells ($r = 0.05$, $n = 20$, $P = 0.83$). In contrast, the metabolic activity increased with uptake for metabolically inactive ($r = 0.61$, $n = 14$, $P = 0.02$) G_2/M cells and

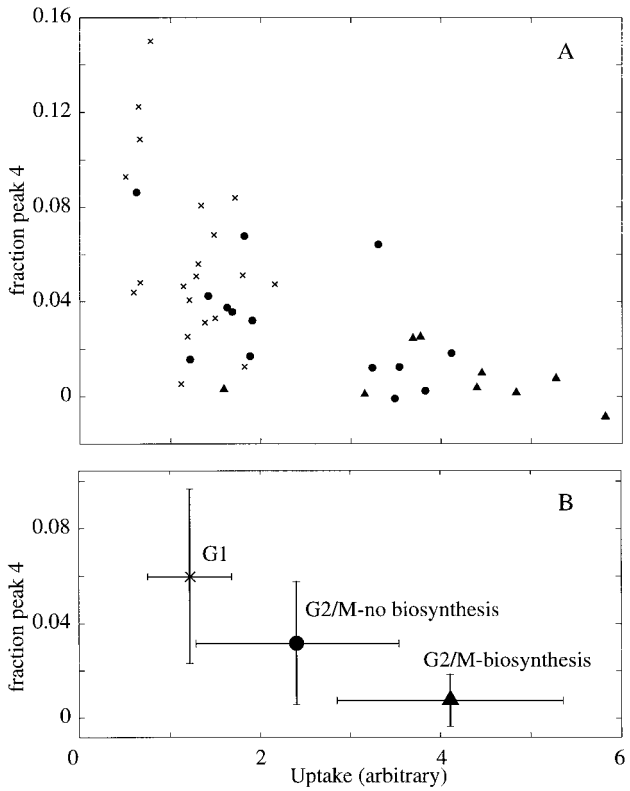

FIG. 5. Correlation of fraction of peak 4 (identified in Fig. 1) in each cell and total substrate uptake. Cells in the G_1 phase are denoted by ×, metabolically inactive G2/M cells are denoted by ●, metabolically active G2/M cells are denoted by ▲. **A:** Scatter plot. **B:** Average ± 1 SD.

for metabolically active G_2/M cells ($r = 0.84$, $n = 9$, $P = 0.005$). The significant correlation between the substrate uptake and the metabolic activity suggests that the enhanced metabolic activity either activates penetration or retards excretion of TMR-labeled species through the cellular membranes.

DISCUSSION

Metabolism is the total set of chemical reactions that occur in a cell. While classic analytical tools, such as chromatography and electrophoresis, can provide detailed information on metabolic pathways (28,34), they provide no information on the range of activity within a cellular population; differentiation in a population is not discernable in these assays. In contrast, cytometric assays, such as flow or image cytometry, generate a powerful correlation between cell markers and the activity of a single enzyme (35,36). However, the assays neither provide information on metabolic pathways and fluxes nor discriminate between substrate uptake and enzyme activity.

We used metabolic cytometry to study the metabolism of single cells as a function of cell cycle. The biosynthetic and biodegradation behavior of cells varies during the cell cycle. About 40% of the cells in the G_2/M phase actively accumulate the biosynthetic products. The biosynthetically active cells generate either Le^X or Le^Y, but not both.

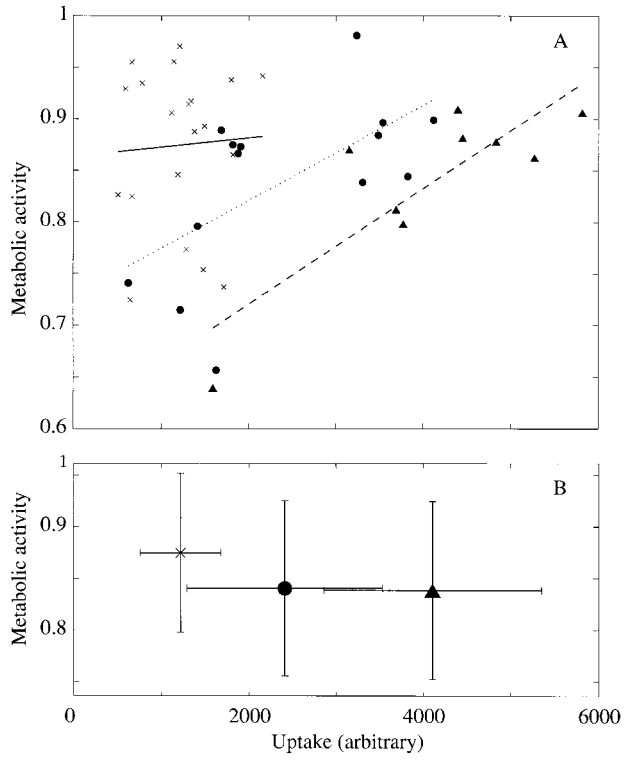

FIG. 6. Correlation of metabolic activity and substrate uptake. Cells in the G_1 phase are denoted by ×, metabolically inactive G2/M cells are denoted by ●, metabolically active G_2/M cells are denoted by ▲. **A:** Scatter plot. The solid line is the least-squares fit of a line to the G_1 data. The dotted line is the least squares fit of a line to the metabolically inactive G_2/M cells. The dashed line is the least-squares fit of a line to the metabolically active G2/M cells. **B:** Average ± 1 D.

The biosynthesis of Le^X and Le^Y from LacNAc is mediated by a set of fucosyltransferases

$$\text{LacNAc} \xrightarrow{\alpha(1\rightarrow2)\text{FucT}} \text{H-type II} \xrightarrow{\alpha(1\rightarrow3)\text{FucT}} Le^Y.$$

Le^Y is formed by sequential action of the α1→2 fucosyltransferase to form the intermediate H-type II trisaccharide, followed by the α1→3 fucosyltransferase to form Le^Y. We saw no evidence for the H-type II intermediate, which suggests that the α1→3 fucosylation of H-type II was much faster than the α1→2 fucosylation of LacNAc. The biosynthesis of Le^X proceeds by α1→3 fucosylation of LacNAc.

$$\text{LacNAc} \xrightarrow{\alpha(1\rightarrow3)\text{FucT}} Le^X.$$

Once Le^X is formed, it cannot be converted to Le^Y because it is not a substrate for known mammalian α1→2 fucosyltransferases. The observation of either Le^X or Le^Y implies that all biosynthetically active cells contain the α1→3 fucosyltransferase. The failure to observe both Le^X and Le^Y results from the strict specificity of the α1→2 fucosyltransferase. Those cells that express this enzyme generate Le^Y by way of the H-type II intermediate, whose fleeting existence was not detected in our experiments. Those cells that produce Le^X lack α1→2 fucosyltransferase or contain much higher levels of lack α1→3 fucosyltransferase.

In contrast, oligosaccharide biosynthesis appears to be shut off during the G_1 phase; we observed no biosynthesis in these cells. Higher level of glycosylation activity during the G_2/M phase in HT29 cells was earlier demonstrated using bulk analysis of synchronized cells (39). Further studies will be required to determine if Le^X or Le^Y produced during the G_2/M phase is excreted or biodegraded before the cell enters the G_1 phase. At present, we do not have enough information for extensive speculation on the reasons for differences in glycosylation metabolism between G_1 and G_2/M cells. One possible explanation may be that glycosylation of the cytoskeletal proteins is involved in structural rearrangements during the G_2/M phase.

CONCLUSIONS

We demonstrate the first use of ultrasensitive laser-induced fluorescence with a high-resolution separation by capillary electrophoresis to monitor biosynthetic and biodegradation pathways within single cells. The biotransformations were correlated with cell cycle by measuring DNA ploidy before the electrophoresis analysis.

Cells are divided into several classes. Cells in the G_1 phase had the lowest substrate uptake and were biosynthetically inactive. Roughly half the cells in the G_2/M phase were biosynthetically active; they had the highest substrate uptake and the highest metabolic activity. Biosynthetically inactive G_2/M cells were intermediate in their properties.

These data provide correlations in the activity of different enzymes within the cell, substrate uptake, and cell cycle. The regulation of the molecular machinery associated with oligosaccharide metabolism undoubtedly will change in response to differentiation and environment; the tools presented here can be used to study these changes.

Metabolic cytometry will be useful whenever a cell takes up a fluorescent enzymatic substrate. For example, we have generated metabolic profiles based on the disaccharide βGal(1→3)βGlcNAc-TMR metabolism in A431 human epidermoid cancer cells and on the trisaccharide αGlc(1→2)αGlc(1→3)αGlc-TMR metabolism in yeast spheroplasts (37). The last example points out one limitation of metabolic cytometry — cells must lyse under the experimental conditions. The cell wall of yeast is robust in our buffer so spheroplasts were prepared to facilitate lysis. However, all mammalian cell lines that we have tested are lysed within 1 min.

Metabolic cytometry will be valuable in studying the mechanisms of metabolism. For example, a fluorescent substrate like that used in this report could be used to study neoplastic transformations, which often have altered glycosyltransferase activity (38). This technology can be expanded to use any of the dyes employed in image cytometry. For example, labeled antibodies can be used to

monitor cell surface marker expression, which can then be correlated with oligosaccharide metabolism. Similarly, other metabolic pathways can be monitored and correlated with cell surface marker expression or phase of cell cycle.

The technique is presently limited by low throughput; about 15 min are required to analyze each cell. Although the technology may be improved, the throughput of chemical cytometry is unlikely to approach the throughput of conventional cytometry. However, the high information content of the signal will be of value, particularly when details of enzymatic cascades are to be studied. Rather than averaging response over a cellular population, specific subpopulations can be identified and characterized. The technology will be particularly important in embryogenesis and in fine-needle aspirants, when relatively few cells are available for analysis.

ACKNOWLEDGMENTS

This work was funded by Research Grants from the Natural Sciences and Engineering Research Council to M.M.P. and N.J.D. The authors would like to thank Dr. R. Bhatnagar, Mrs. D. Rutkowsky and Mrs. J. Wizniak for technical assistance in confocal microscopy and flow cytometry.

LITERATURE CITED

1. Edstrom JE. Nucleotide analysis on the cyto-scale. Nature 1953;172: 908.
2. Maholi GT, Niewisch HB. Electrophoresis of hemoglobin in single erythrocytes. Science 1965;150:1824–1826.
3. Kennedy RT, St. Claire RL, White JG, Jorgenson, JW. Chemical analysis of single neurons by open tubular liquid chromatography. Mikrochim Acta 1987;II: 37–45.
4. Kennedy RT, Oates MD, Cooper BR, Nickerson B, Jorgenson JW. Microcolumn separations and the analysis of single cells. Science 1989;246:57–63.
5. Wallingford RA, Ewing AG. Capillary zone electrophoresis with electrochemical detection in 12.7 microns diameter columns. Anal Chem 1988;60:1972–1975.
6. Kristensen HK, Lau YY, Ewing AG. Capillary electrophoresis of single cells: observation of two compartments of neurotransmitter vesicles. J Neurosci Meth 1994;51:183–188.
7. Gilman SD, Ewing AG. Analysis of single cells by capillary electrophoresis with on-column derivatization and laser-induced fluorescence detection. Anal Chem 1995;67:58–64.
8. Colliver TL, Brummel CL, Pacholski ML, Swanek FD, Ewing AG, Winograd N. Atomic and molecular imaging at the single-cell level with TOF-SIMS. Anal Chem 1997;69:2225–2231.
9. Hsieh S, Dreisewerd K, van der Schors RC, Jimenez CR, Stahl-Zeng J, Hillenkamp F, Jorgenson JW, Geraerts WP, Li KW. Separation and identification of peptides in single neurons by microcolumn liquid chromatography-matrix-assisted laser desorption/ionization time-of-flight mass spectrometry and postsource decay analysis. Anal Chem 1998;70:1847–1852.
10. Fuller RR, Moroz LL, Gillette R, Sweedler JV. Single neuron analysis by capillary electrophoresis with fluorescence spectroscopy. Neuron 1998;20:173–181.
11. Chen G, Ewing AG. Chemical analysis of single cells and exocytosis. Crit Rev Neurobiol 1997;11:59–90.
12. Lillard SJ, Yeung ES, Lautamo RM, Mao DT. Separation of hemoglobin variants in single human erythrocytes by capillary electrophoresis with laser-induced native fluorescence detection. J Chromatogr 1995; 718:397–404.
13. Cheung NH, Yeung ES. Distribution of sodium and potassium within individual human erythrocytes by pulsed-laser vaporization in a sheath flow. Anal Chem 1994;66:929–936.
14. Lee TT, Yeung ES. Quantitative determination of native proteins in individual human erythrocytes by capillary zone electrophoresis with laser-induced fluorescence detection. Anal Chem 1992;64:3045–3051.
15. Xue Q, Yeung ES. Determination of lactate dehydrogenase isoenzymes in single lymphocytes from normal and leukemia cell lines. J Chromatogr 1996;677:233–240.
16. Huang L, Shen H, Atkinson MA, Kennedy RT. Detection of exocytosis at individual pancreatic beta cells by amperometry at a chemically modified microelectrode. Proc Natl Acad. Sci. (USA) 1995;92:9608–9612.
17. Paras CD, Kennedy RT. Electrochemical detection of exocytosis at single rat melanotrophs. Anal Chem 1995;67:3633–3637.
18. Orwar O, Jardemark K, Jacobson I, Moscho A, Fishman HA, Scheller RH, Zare RN. Patch-clamp detection of neurotransmitters in capillary electrophoresis. Science 1996;272:1779–1782.
19. Chiu DT, Lillard SJ, Scheller RH, Zare RN, Rodriguez-Cruz SE, Williams ER, Orwar O, Sandberg M, Lundqvist JA. Probing single secretory vesicles with capillary electrophoresis. Science 1998; 279:1190–1193.
20. Tong W, Yeung ES. On-column monitoring of secretion of catecholamines from single bovine adrenal chromaffin cells by capillary electrophoresis. J Neurosci Meth 1997;76:193–201.
21. Lillard SJ, Yeung ES. Temporal and spatial monitoring of exocytosis with native fluorescence imaging microscopy. J Neurosci Meth 1997;75:103–109.
22. Lillard SJ, Yeung ES, McCloskey MA. Monitoring exocytosis and release from individual mast cells by capillary electrophoresis with laser-induced native fluorescence detection. Anal Chem 1996;68:2897–2904.
23. Tong W, Yeung ES. Monitoring single-cell pharmacokinetics by capillary electrophoresis and laser-induced native fluorescence. J Chromatogr 1997;689:321–325.
24. Basile F, Beverly MB, Abbas-Hawks C, Mowry CD, Voorhees KJ, Hadfield TL. Direct mass spectrometric analysis of in situ thermally hydrolyzed and methylated lipids from whole bacterial cells. Anal Chem 1998;70:1555–1562.
25. Easterling ML, Colangelo CM, Scott RA, Amster IJ. Monitoring protein expression in whole bacterial cells with MALDI time-of-flight mass spectrometry. Anal Chem 1998;70:2704–2709.
26. Whittal RM, Keller BO, Li L. Nanoliter chemistry combined with mass spectrometry for peptide mapping of proteins from single mammalian cell lysates. Anal Chem 1998;70:5344–5347.
27. Le XC, Zhang Y, Dovichi NJ, Compston CA, Palcic MM, Beever RJ, Hindsgaul O. Study of the enzymatic transformation of fluorescently labeled oligosaccharides in human epidermoid cells using capillary electrophoresis with laser-induced fluorescence detection. J Chromatogr 1997; 781:515–522.
28. Zhang Y, Le X, Dovichi NJ, Compston CA, Palcic MM, Diedrich P, Hindsgaul O. Monitoring biosynthetic transformations of *N*-acetyllactosamine using fluorescently labeled oligosaccharides and capillary electrophoretic separation. Anal Biochem 1995;227:368–376.
29. Le X, Scaman C, Zhang Y, Zhang J, Dovichi NJ, Hindsgaul O, Palcic MM. Analysis by capillary electrophoresis-laser-induced fluorescence detection of oligosaccharides produced from enzyme reactions. J Chromatogr 1995; 716:215–220.
30. Zhao JY, Dovichi NJ, Hindsgaul O, Gosselin S, Palcic MM. Detection of 100 molecules of product formed in a fucosyltransferase reaction. Glycobiology. 1994;4:239–242.
31. Cheng YF, Dovichi NJ. Subattomole amino acid analysis by capillary zone electrophoresis and laser-induced fluorescence. Science 1998; 242:562–564.
32. Wu S, Dovichi N.J. High-sensitivity fluorescence detector for fluorescein isothiocyanate derivatives of amino acids separated by capillary zone electrophoresis J Chromatogr 1989;480:141–155.
33. Chen DY, Dovichi, NJ Single-molecule detection in capillary electrophoresis: molecular shot noise as a fundamental limit to chemical analysis. Anal Chem 1996;68:690–696.
34. Sugino Y, Teraoka H, Shimono H. Metabolism of deoxyribonucleotides. I. Purification and properties of deoxycytidine monophosphokinase of calf thymus. J Biol Chem 1966;241:961–969.
35. Dive C, Workman P, Watson JV. Improved methodology for intracellular enzyme reaction and inhibition kinetics by flow cytometry. Cytometry 1987;8:552–561.
36. Yashphe J, Halvorson OH. β-D-Galactosidase activity in single yeast cells during cell cycle of *Saccharomyces lactis*. Science 1976;191: 1283–1284.
37. Le XC, Tan W, Scaman C, Szpacenko A, Arriaga E, Zhang Y, Dovichi NJ, Hindsgaul O, Palcic MM. Single cell studies of enzymatic hydrolysis of a tetramethylrhodamine labeled trisaccharide in yeast. Glycobiology 1999;9:219–225.
38. Hakomori, S. Aberrant glycosylation in tumors and tumor-associated carbohydrate antigens. Advan Cancer Res 1989;52:257–331.
39. Chou CF, Omary M. Mitotic arrest-associated enhancement of O-linked glycosylation and phosphorylation of human keratins 8 and 18. J Biol Chem 1993;268:4465–4472.